Annual variability of mesospheric CO measured by a ground-based FT spectrometer : comparisons with Odin/SMR anda 2 model.

N.B. Jones, Y. Kasai, E. Dupuy, Y. Murayama, Brice Barret, M. Sinnhuber, A. Kagawa, T. Koshiro, Jakub Urban, P. Ricaud, et al.

Stratomesospheric CO measured by a ground-based Fourier Transform Spectrometer over Poker Flat, Alaska: Comparisons with Odin/SMR and a 2-D model

N. B. Jones,[1] Y. Kasai,[2] E. Dupuy,[3,4] Y. Murayama,[2,5] J. Urban,[6] B. Barret,[7] M. Sinnhuber,[8] A. Kagawa,[2,9] T. Koshiro,[10] P. Ricaud,[7] and D. Murtagh[6]

Received 13 August 2006; revised 18 May 2007; accepted 22 June 2007; published 20 October 2007.

[1] The interseasonal variability of stratomesospheric CO is reported from Poker Flat, Alaska, using spectra from a ground-based Fourier Transform Spectrometer (gb-FTS) for the time period from 2000 to 2004. The CO spectra were analyzed using an optimal estimation technique that separates the tropospheric and stratospheric/mesospheric components into partial columns. The distribution of CO in the polar winter is such that the gb-FTS retrieved partial column is weighted to the mesosphere. The gb-FTS data are compared with measurements of partial column CO from the Sub-Millimeter Radiometer on board the Odin satellite and shown to be in very good agreement despite the relatively small sample size. The mean difference of the two data sets indicates a small positive bias (7.6 ± 6%) in favor of the Odin data, with a correlation coefficient, $r^2 = 0.91$. The gb-FTS data indicate that there is a strong seasonal dependence of the CO partial column that is consistent with known winter polar thermospheric descent of CO enriched air. Year-to-year variability is explained in terms of mesospheric wind dynamics, which show 2004 and components of 2002 were affected by earlier than expected breakdown (30 ± 13 d) of the winter polar circulation compared with 2000 to 2003. Finally, the measured CO data is compared with a 2-D chemical transport model that gives support to the idea that springtime polar mesospheric CO is driven by meridional winds.

Citation: Jones, N. B., et al. (2007), Stratomesospheric CO measured by a ground-based Fourier Transform Spectrometer over Poker Flat, Alaska: Comparisons with Odin/SMR and a 2-D model, *J. Geophys. Res.*, *112*, D20303, doi:10.1029/2006JD007916.

1. Introduction

[2] Carbon monoxide (CO) has been used as a tracer for global-scale transport in the middle atmosphere [see, e.g., *Solomon et al.*, 1985; *Allen et al.*, 1999]. Its long photochemical lifetime, coupled with strong concentration gradients, makes CO an excellent tracer for estimating air mass descent rates in the polar stratosphere and lower mesosphere. Until recently, there have been few reports of mesospheric CO observations in the literature, the majority of which have been made by ground-based microwave radiometers [*Bevilacqua et al.*, 1985; *Aellig et al.*, 1995]. The Improved Stratospheric and Mesospheric Sounder (ISAMS) aboard the Upper Atmosphere Research Satellite (UARS) reported the global distribution of stratomesospheric CO over a 6-month observation period from 1991 to 1992 [*López-Valverde et al.*, 1996; *Allen et al.*, 1999].

[3] Mesospheric CO observations have been reported from September 2000 to September 2002 over the Onsala Space Laboratory, Sweden (57.4°N, 12°E) [*Forkman et al.*, 2003, 2005], where the correlation of the CO amount with water vapor was noted. There have been a number of satellite reports, for example, the Sub-Millimeter Radiometer on board the Odin satellite (hereafter referred to as Odin/SMR) [*Dupuy et al.*, 2004] measured the day/night concentrations of stratomesospheric CO. The ACE-FTS sensor [*Clerbaux et al.*, 2005; *Jin et al.*, 2005], the Interferometric Monitor of Greenhouse gases (IMG) which flew on board the Japanese ADEOS platform in 1996–1997 [*Barret et al.*, 2005], and quite recently [*Ahmad et al.*, 2006] the AURA/MLS platform have all reported CO measurements. These satellite data have been successfully validated against each other and agree very well [*Jin et al.*, 2005; *Barret et al.*, 2006]. The first mesospheric detection of CO

[1]School of Chemistry, University of Wollongong, Wollongong, New South Wales, Australia.
[2]Environmental Sensing and Network Group, Applied Electromagnetic Research Center, National Institute of Information and Telecommunications Technology, Tokyo, Japan.
[3]Observatoire Aquitain des Sciences de l'Univers, Floirac, France.
[4]Now at Institute of Space and Atmospheric Studies, University of Saskatchewan, Saskatoon, Saskatchewan, Canada.
[5]Also at National Institute of Polar Research, Tokyo, Japan.
[6]Department of Radio and Space Science, Chalmers University of Technology, Gothenburg, Sweden.
[7]Laboratoire d'Aérologie, UMR 5560 CNRS, Universite Paul Sabatier, Observatoire de Midi-Pyrénées, Toulouse, France.
[8]Institute of Environmental Physics, University of Bremen, Bremen, Germany.
[9]Fujitsu FIP Corporation, Tokyo, Japan.
[10]Research Institute for Sustainable Humanosphere, Kyoto University, Uji, Japan.

0148-0227/07/2006JD007916

from gb-FTS spectral measurements was reported by *Kasai et al.* [2005a]. Ground-based FTS measurements of stratospheric/mesospheric CO partial columns (hereafter referred to as smCO) from several sites in the Arctic, Northern and Southern midlatitudes, and Antarctica has recently been reported and compared with model studies [*Velazco et al.*, 2007]. In this current paper, the work of *Kasai et al.* [2005a] is expanded to cover the time period from 2001 to 2004 and compared with colocated measurements from the Odin satellite [*Dupuy et al.*, 2004], the season to season variability of the smCO partial column above 24 km is investigated in terms of the dynamics of the Arctic polar circulation, and finally a 2-D model simulation is used to help confirm the relationship between the meridional wind circulation and the measured CO column. Since Poker Flat is often located outside of the stratospheric polar vortex, it is well suited to the study of the effects of meridional winds on the CO column. While this phenomenon is well known, this paper presents the first observational evidence of year-to-year variability in the relationship between mesospheric CO and wind dynamics. This wind/transport variability also has consequences on the distribution of other trace gases in the atmosphere.

[4] We consider that the meridional winds are most likely the driver of CO transport; on a mesospheric global scale, zonal and meridional winds must behave in a dynamically consistent manner. That is, in general gravity wave drag decelerates the upper part of the mesospheric jet structure. This leads to meridional circulation from the summer to winter pole, with a predominance of westerly winds. This corresponds to meridional flow toward the winter pole in the upper mesosphere. CO is likely transported toward the Northern Hemisphere polar region when the winter mesosphere is dominated by westerly winds. In this paper we use zonal winds as a proxy for the meridional wind flow. Why we argue that this is a reasonable assumption is discussed in detail in sections 3.4 and 3.5.

[5] The paper is organized as follows: The background on observations from the gb-FTS, Odin/SMR, and MF radar measurements are described in sections 2.1, 2.2, and 2.3, respectively, while the 2D model is briefly described in section 2.4. The results and discussion are presented in section 3, which consists of detailed discussion on the Poker Flat gb-FTS column data in section 3.1, the Odin/SMR data in section 3.2, a quantitative comparison between the gb-FTS and Odin/SMR data in section 3.3, the MF radar data in section 3.4, the Leeds-Bremen model in section 3.5, a discussion on the 2003–2004 Arctic winter in section 3.6, and finally a comparison of the 2003–2004 Arctic winter with earlier years with respect to the behavior of the Poker Flat CO columns in section 3.7.

2. Observation

[6] The Poker Flat gb-FTS is one of the instruments that is part of the recently completed "Alaska Project", a joint research project between the National Institute of Information and Telecommunications Technology (NICT) of Japan and the Geophysical Institute of the University of Alaska, Fairbanks [*Iishi et al.*, 2000]. The Poker Flat gb-FTS (a Bruker 120HR, resolution 0.0035 cm^{-1}) was installed in September 1999. The site is located at the Poker Flat Research Range (PFRR: Altitude 0.61 km; latitude 65.11°N; longitude 147.42°W). The instrument is equipped with both InSb and MCT liquid nitrogen cooled detectors and a KBr beam splitter. Optical filters limit the spectral band pass to the 1850–2100 cm^{-1} region that includes the strong (1–0) CO fundamental vibrational band. Further details on the instrument and data system has already been described in some detail [*Kasai et al.*, 2005a, 2005b] and will not be repeated here. However, some comments in regard to the analysis method will be given, as this is relevant to the particular problem of retrieving trace gases from the stratosphere/mesosphere.

2.1. IR Spectroscopic Analysis

[7] The forward and inverse models used in this study are detailed in the paper by *Kasai et al.* [2005a]. The CO abundance determination, profiles, and characterization of the inversions were computed using the established SFIT2 (version 3.8) algorithm [*Rinsland et al.*, 1998], which is based on the Optimal Estimation Method (OEM) of *Rodgers* [2000]. While the CO retrieval analysis followed previous methods outlined by *Rinsland et al.* [1998] which simultaneously fitted the strong R_3 fundamental line of ^{12}CO at 2158.2997 cm^{-1}, along with the two weak isotopic P_{10} and P_7 lines of ^{13}CO at 2057.8578 cm^{-1} and 2069.6559 cm^{-1}, respectively, there were several notable differences in the *Kasai et al.* [2005a] analysis. Our interest in the CO profile, in this study, is focused on the stratosphere-mesosphere. The P_{10} and P_7 lines are relatively weak (absorption depths of order 20%) compared to the strong R_3 line, which is saturated at its centre. The information content in these absorption features is such that the weaker lines contain most if not all information in the upper troposphere and above. The R_3 line on the other hand is heavily weighted to the bottom few kilometers. We also weighted these weaker lines by setting the measurement error covariance a factor of 5 lower within 0.2 cm^{-1} of the P_7 and P_{10} line centers, which would have the same effect of increasing the signal to noise ratio 5 times higher in this narrow 0.2 cm^{-1} frequency range. This particular detail in the retrieval process of appropriately weighting spectral points at the Doppler core of the weak CO lines is the important step in the inverse method that avoids instabilities in the broader spectrum (from various error sources discussed below) that would otherwise make a successful determination of the stratomesospheric column very difficult. All terrestrial CO lines suffer interference to varying degrees from solar CO, so a fourth window from 2112.08–2112.18 cm^{-1} was added that included an isolated solar CO line. As pointed out in the paper by *Kasai et al.* [2005a], the forward model also assumes local-thermodynamic-equilibrium (LTE). Non-LTE effects are important for the CO (1–0) band above about 40 km, [*López-Valverde et al.*, 1996]. However, the effects on both the chemistry [*Müller et al.*, 1996] and photodissociation [*Bhattacharya et al.*, 2000] on the minor isotopic species of CO is less than 5% and 1%, respectively.

[8] Another important consideration is the lower-altitude limit at which CO from the upper atmosphere contributes to the CO absorption feature. From this determination, the altitude range over which partial columns will be computed is set. After taking into account the Full Width Half

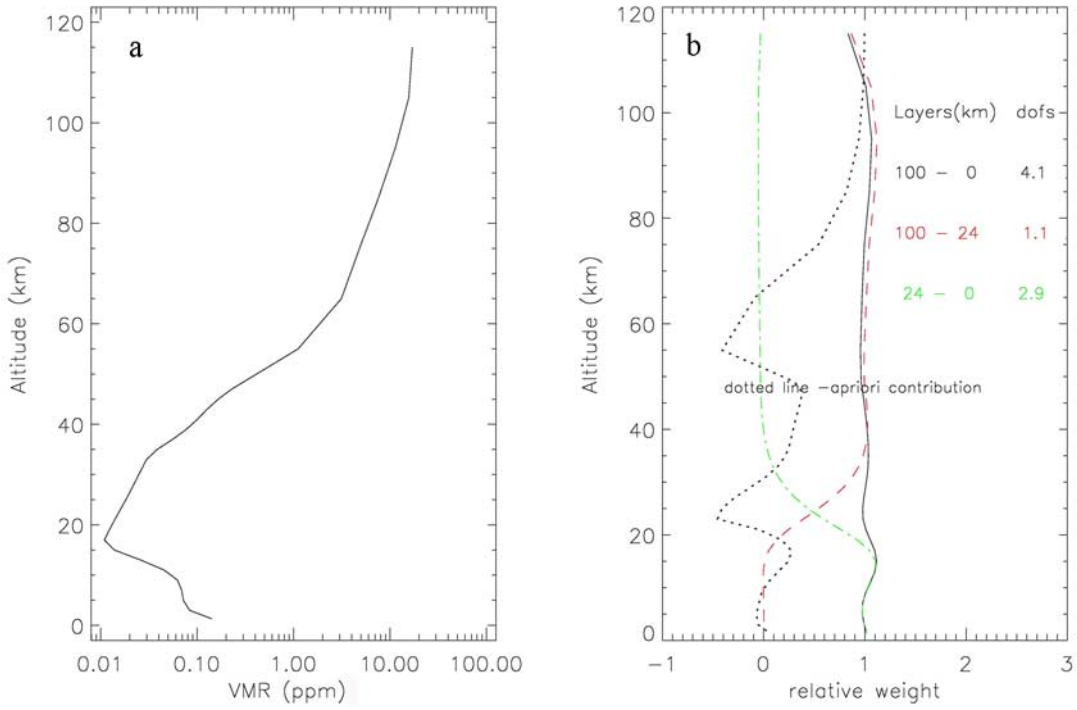

Figure 1. (a) A priori CO mixing ratio profile used in the analysis and (b) averaging kernels for the three layers 0–100 km (black solid line), 0–24 km (red dashed line), and 24–100 km (green dash-dotted line).

Maximum (FWHM) of a measured spectrum (0.003–0.0035 cm^{-1}), the instrumental resolution of 0.0035 cm^{-1} as set by the maximum optical path difference of 258 cm, and the theoretical width of the $^{13}CO(P_{10}, P_7)$ lines in the stratosphere (0.0027 cm^{-1} for a typical range of temperatures over Poker Flat), *Kasai et al.* [2005a] determined a lower altitude of approximately 27 km would be consistent with the instrumental line width. The final choice of altitude range though also took into consideration the information content and geometric shape of computed averaging kernels.

[9] Seasonal CO a priori profiles were used in the analysis based on a zonal mean average measurement covering the latitude range from 70–80°N [*Dupuy et al.*, 2004]. From this original profile, subsequent profiles were developed that gave the best fit in the core of CO lines using a subset of spectra. For other interfering species, their a priori mixing ratio profiles were obtained from fitted retrieved profiles from isolated spectral bands at 3035 cm^{-1} and 2482 cm^{-1} for O_3, and N_2O, respectively. The water vapor profile was based on sonde measurements obtained over Fairbanks. The covariance matrix for the CO a priori uncertainties was diagonal; below the tropopause (assumed to be constant at 8 km), the a priori uncertainty was set to 0.22 increasing to 0.55 at 20 km, staying constant at this value to the top of the model atmosphere (100 km). For the other interfering species, an uncertainty of 1.0 (or 100%) was used since a single scaling factor was adjusted for their respective concentration profiles. The HITRAN 2000 line list [*Rothman et al.*, 2003] was used consistently for all spectroscopic analyses. Temperature and pressure profiles were obtained from daily 16:00 NCEP measurements, and smoothly connected to the 1976 US Standard Atmosphere.

[10] Figure 1 illustrates the resulting averaging kernels for this combination of lines, and inverse model parameters with the altitude ranges chosen to give best separation of the partial columns consistent with the previous discussion of upper atmospheric CO contribution for a CO a priori profile for the month of April. The total column is evenly weighted throughout the atmosphere, while a partial column from 24 to 100 km gives good separation between the stratosphere-mesosphere and the lower stratosphere. Figure 1 also shows the relative contribution of the CO a priori to the retrieved profile (black dotted line). Good sensitivity occurs when the CO a priori contribution is near zero, while numbers approaching unity indicate that information is coming solely from the a priori. In this particular case, it can be seen that at most altitudes up to about 80 km there is reasonable sensitivity to the spectrum. Also indicated in the key of Figure 1 are the degrees of freedom for signal (dofs) for each layer, another indication of the information content [*Rodgers*, 2000]. There are 4 independent pieces of information contained in the total column (since the ground to 100 km layer has a dofs of 4.0), and of this information, 1.1 pieces are located in the partial column from 24 to 100 km.

[11] The layer scheme adopted in the model atmosphere used a 2 km grid up to 50 km, and 10 km above this to the top of the model atmosphere at 100 km. In Figure 1, for the purposes of illustrating the sensitivity of the averaging kernel above our model atmosphere, the grid was extended to 120 km. However, the contribution to the CO partial column between 24 and 100 km is less than 1% if this

partial column is extended to 120 km. In terms of the percent fraction of the total column for each partial column, the partial column from 24 to 100 km is 3.3% of the total column (and therefore 0–24 km is 96.7%). For the different atmospheric regimes, the troposphere is 95.4%, stratosphere 2.4%, mesosphere 2.1% and thermosphere less than 0.05%.

[12] The error budget for the CO retrieval was estimated using the technique outlined by *Rodgers* [2000, chapter 3.2, equations (3.17), (3.18), and (3.19)] for the smoothing error (S_n), forward model parameter error, and statistical measurement noise (S_m), respectively. For the case of temperature errors (S_t), since the a priori model atmosphere is precomputed in SFIT2, but also decoupled from the main forward model, the weighting functions for temperature were computed by repeated perturbation to the temperature profile and retrieval of the subsequent CO profile. In doing so, the contribution function for temperature was built up over all 29 atmospheric layers. To realize the final temperature error term, the error covariance matrix was estimated using 1 a of temperature data. Similarly, the spectroscopic model parameter error (which included the line strength and width) were estimated by perturbing the respective spectroscopic line parameter and comparing the retrieved column with the unperturbed case. On the basis of this process, the total error for the smCO partial column reported here is estimated to be 13%, which consists of random error of 8% (with components containing measurement (S_m = 5%), smoothing (S_n = 8%) and temperature (S_t = 1%) errors) and systematic error of 10% (with components containing spectroscopic (2%), instrumental (1%) and a priori profile (9%)).

2.2. Odin Satellite Measurements

[13] The Odin SMR instrument is the first submillimeter wave instrument sounding the Earth atmosphere from space. It is equipped with four tunable heterodyne receivers in the frequency range 486–580 GHz that perform day and night limb measurements using thermal emission from trace constituents. CO is one of the target species with an intense line at 578.628 GHz [*Murtagh et al.*, 2002]. The measurements of CO have continued since October 2003 on 1–2 observation days per month, time-shared with other aeronomy and astronomy observation modes. The details of the CO retrieval process, the performance of the observations, and error considerations have been presented previously [*Dupuy et al.*, 2004]. The Odin/SMR instrument has enough sensitivity to observe CO in the altitude region from 17–110 km, with a vertical resolution of 3–4 km [*Dupuy et al.*, 2004]. The SMR CO profiles used in this work were produced from version 225 by the French Odin level-2 processor CTSO (Chaine du Traitement Scientifique Odin). The main difference between this present data and the earlier version 223 reported by *Dupuy et al.* [2004] is that temperature is no longer retrieved simultaneously with CO and O_3 [*Barret et al.*, 2006]. The single scan precision for CO is better than 25 ppb in the stratosphere, increasing to 2 ppm at the top of the mesosphere. A detailed description of all error sources is given by *Dupuy et al.* [2004]; the error ranges from 15 to 50% depending on the CO concentration. For smCO partial columns, the error translates to 5 to 30% depending on the CO amount, the lower error occurring in the polar winter when the CO amounts are large.

[14] CO observed by Odin/SMR has been compared with measurements from other space platforms such as ACE and Aura/MLS [*Jin et al.*, 2005; *Barret et al.*, 2006], and also with model calculations [*Dupuy et al.*, 2004; *Jin et al.*, 2005]. Odin/SMR compared very well with ACE profiles from the lower stratosphere to the thermosphere, generally to within their respective uncertainties. Both Odin/SMR and ACE have similar biases when compared to Aura/MLS ranging from 50 to 250% at varying altitudes and latitudes due to known artifacts in the MLS processing [*Barret et al.*, 2006]. Because of this known publication record, in this paper we have used CO from Odin/SMR as reference data. While Odin reports CO profiles and can derive a column (see section 3.2), gb-FTS measurements normally report CO columns (and can subsequently derive a CO profile). The nature of the analysis techniques, instruments, platforms and geometries mean that the two data sets are not directly comparable. We have therefore used the method outlined by *Rodgers and Connor* [2003]. For simplicity, since the Odin measurement is of much higher vertical resolution, we assume this to be the "truth", against which the gb-FTS measurement is compared. We can therefore write the following expression, following the nomenclature of *Rodgers and Connor* [2003], that relates the lower-resolution gb-FTS column with the higher-resolution Odin derived column:

$$\tilde{C}_{fo} = C_c + a_f^T(\tilde{x}_o - x_c) \quad (1)$$

where $\tilde{C}_{fo}$ is the smoothed Odin column, C_c the ensemble Odin column average, a_f^T the transpose of the gb-FTS column averaging kernel, $\tilde{x}_o$ the Odin mixing ratio profile, and x_c the Odin ensemble average mixing ratio profile. The Odin ensemble average was taken as the mean of all Odin data. Odin columns were computed from the measured profile by first regridding the Odin CO mixing ratios onto the gb-FTS 29 layer vertical grid, and then summing up the 29 discrete CO densities as determined from predefined air mass computations. The air masses were determined from the algorithm used as part of the ray tracing component of SFIT2. The nominal scan-range of the Odin/SMR measurement is 7–110 km, while information can be retrieved from 18–20 km up to 100–110 km. The above regridding operation computes the Odin partial column, smoothed by the gb-FTS averaging kernel, over the same altitude range as the gb-FTS measurement, i.e., from 24 to 100 km.

2.3. Poker Flat MF Radar

[15] The MF radar has been operating at Poker Flat since 1998 to observe mesospheric zonal (east-west) and meridional (north-south) wind velocities in the altitude range of approximately 60–90 km. The instrumentation is described in more detail elsewhere [see, e.g., *Murayama et al.*, 2000]. The altitude resolution is 4 km (oversampled every 2 km). Wind estimation is by full correlation analysis (FCA) [e.g., *Briggs*, 1984], which is a method to derive horizontal winds from the drift velocity and autocorrelation of ionospheric irregularity signals. The wind data used in this study have a 1 h sampling time, giving an estimated error in the mean wind velocities of 1–2 ms^{-1}. It has been widely accepted that the MF radar technique is an important tool for studying mesospheric dynamics, especially atmospheric

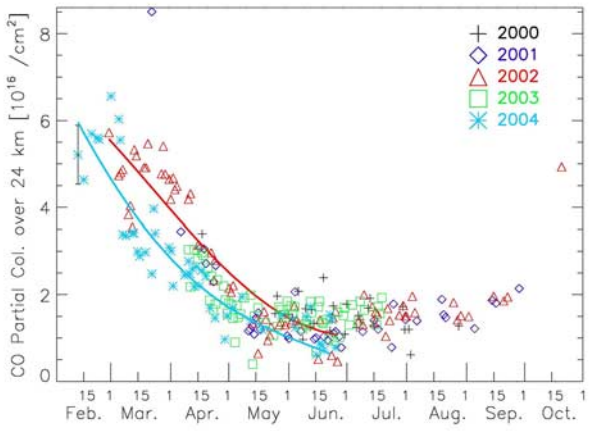

Figure 2. Stratomesospheric column of CO (24–100 km) from the gb-FTS for all data that covers the time period from 2000 to 2004. Different years are indicated by the symbols in the legend. Years 2002 and 2004 are highlighted with solid lines as particular years where the dynamics of the winter to summer transition was different. They were also chosen because of the completeness of their respective samples as a function of date. An indicative vertical error bar is plotted on the first data point of 2004 on the basis of the error budget from section 2.1.

waves and circulation [e.g., *Dowdy et al.*, 2001; *Riggin et al.*, 2003].

2.4. Mesospheric CO Model

[16] CO was simulated using a modified version of the two-dimensional Leeds-Bremen model, a global photolysis, chemistry and transport model of the stratosphere and mesosphere [*Sinnhuber et al.*, 2003]. It is a coupled chemistry-dynamics model which combines the THIN AIR meteorological code [*Kinnersley*, 1996] and the SLIMCAT chemistry code [*Chipperfield*, 1999]. The model calculates temperature, pressure, horizontal and vertical transport, and the behavior of 57 gas-phase and liquid-phase species. CO in this model is assumed to form in the thermosphere, from CO_2 photolysis [see also *Velazco et al.*, 2007], and is transported down into the middle atmosphere during polar winter. In a similar procedure to that outlined in section 2.2, the computed model CO that will be compared with the gb-FTS data was smoothed with the gb-FTS averaging kernel using equation (1).

3. Results and Discussion

3.1. Poker Flats gb-FTS Stratomesospheric Columns

[17] All gb-FTS data for the 2000–2004 period are plotted in Figure 2. Previous studies have reported sections of this data set; *Kasai et al.* [2005a] in a precursor to this paper reported 2 a of data establishing the technique, while more recently *Velazco et al.* [2007] included 2003 and 2004 Poker Flat data in a latitudinal study that included 5 other ground-based sites. In the latter case, the selected partial column covered the altitude range from 18 to 100 km. Shown in Figure 2 is the Poker Flat data set covering the full 5-year interval for the smCO partial column range of 24–100 km.

[18] There are several features in the data that are of note. (1) All 5 a of data show a winter maximum, reduced by a factor of 6 in the summer, (2) the winter-to-summer transition for 2004 occurred approximately 1 month earlier (see discussion below) than in the previous 4 a, (3) on six occasions in March of 2002 (between the 6th and 15th), the smCO partial column followed the 2004 pattern rather than the more general trend of the other years, (4) an examination of the very high smCO partial column on 20 March 2001 (8.5×10^{16} molec cm^{-2}) reveals that the polar vortex was directly over Poker Flat, and (5) the latest data value measured in any one season, 24 October of 2002, indicates that the mesospheric circulation above Poker Flat has returned to a winter pattern.

[19] Our interest in the seasonal differences, as mentioned in point 2 above, lies in the phase difference between 2004 and earlier years. The following functional form was used to obtain trends, phases, and seasonal amplitudes using a gradient expansion algorithm to obtain a nonlinear fit to the gb-FTS data:

$$CO(t) = a_0 + a_1 t + a_2 \cos\left[2\pi\left(t - \phi_y\right)/365\right] \qquad (2)$$

where CO(t) is the CO partial column at time t, a_0 the mean CO partial column at the start of the fitting intervals (2000, 2001.5, and 2003.5), a_1 the linear change in column, a_2 the amplitude in the seasonal modulation and ϕ_y the seasonal cycle phase for year *y*. To fit this data, we combined the data into 3 bands (Table 1) to investigate the early decline in the CO column during the end of 2004, but also to see if there were any statistically significant differences between the period 2000 to 2003 and 2002. The CO in the winter of 2002 appears to decline later compared with other years. Combining data in this fashion also added higher precision to the determination of the yearly phases. As can be seen in Table 1, there is very little difference between the coefficients for bands labeled "1" and "2" as one might expect; the phase difference of 1 week is marginally significant. However, comparing band "3" (winter of 2003/2004) with the earlier years, it is apparent that the phase, in particular, is significantly earlier, $\phi_{2004} = -21 \pm 11$ d (i.e., a peak on 9 December 2003) compared with the 2002 phase, $\phi_{2002} = 9.2 \pm 6$ d (i.e., a peak on 9 January 2002). The time difference between these fitted periods is 30 ± 13 d, i.e., the smCO partial column during the winter of 2003/2004 began declining approximately 1 month earlier than other years. The coefficients for band "2" (2002) and "3" (2004) have been used to plot the two solid lines on Figure 2, the red line for 2000–2003 and blue line for 2004.

3.2. Odin/SMR Partial Columns

[20] Figure 3 shows the CO stratomesospheric partial column from the Odin/SMR instrument for the 2003/2004 period that were recorded within 1000 km of the Poker Flat location. This data is based on the original unsmoothed version 225 CO profiles. The Odin/SMR columns that are directly compared with the gb-FTS columns using the method described in section 2.2 are discussed in section 3.3. The Odin CO profile, errors, measurement response (used as a data quality flag, and set to be >0.75), pressure, and temperature are first interpolated onto a high-resolution grid

Table 1. Fitted Coefficients From Equation (3) for the gb-FTS Data[a]

	Date Sequence	a_0, Constant[b]	a_1, Trend	a_2, Amplitude	Phase, d
1	2000–2003.5	3.4 ± 0.4[c]	−0.02 ± 0.1	2.1 ± 0.3	3.6 ± 5
2	2001.5–2002.8	3.7 ± 0.8	−0.04 ± 0.3	2.5 ± 0.4	9.2 ± 6
3	2003.5–2004.5	4.5 ± 0.7	−0.20 ± 0.4	2.8 ± 0.7	−21 ± 11

[a]The data have been sectioned into the three date sequences (1, 2, and 3) as indicated in the first column. The sequences 2 and 3 were used in Figure 2 to indicate the phase difference between the winters of 2002 and 2004.
[b]The terms a_0, a_1, and a_2 are the coefficients from fitting equation (3).
[c]All coefficients, other than the phase, are in units of 10^{15} molecules cm^{-2}.

(100 m steps). The partial column, from 24–100 km, is then computed from these "high-resolution" profiles. Errors are additionally multiplied with the square root of the ratio of Odin altitude grid step and high-resolution altitude grid step (since statistical noise should be higher on the high-resolution grid). The symbols in Figure 3 are also color coded to represent Modified Potential Vorticity (MPV) values as defined by *Lait* [1994]

$$MPV = PV(\theta/475)^{-9/2} \tag{3}$$

on the 1250 K potential temperature surface (equivalent to approximately 40 km) obtained from the European Centre for Medium Range Weather Forecasting. The red, black, and blue symbols represent PV values > 40 (inside vortex), 30 < PV < 40 (vortex edge), and PV < 30 (outside vortex) all in units of 10^{-6} m^2 s^{-1} kg^{-1} K, respectively. The purpose of displaying the "raw" Odin/SMR columns in Figure 3 is to primarily assist in interpreting later figures and show the relatively minor effect of the smoothing procedure from the gb-FTS averaging kernel (Figure 4). The data in Figure 3 clearly shows the polar winter maximum, coincident with polar vortex air being present in the lower mesosphere, while lower-CO columns in the summer period occur when PV values are also lower.

3.3. A Comparison of gb-FTS and Odin/SMR CO Columns

[21] The stratomesospheric partial column (24–100 km) above Poker Flat for 2004 retrieved from the gb-FTS system (colored diamonds) are plotted in Figure 4, top, along with colocated (criteria of ±5 degrees latitude and ±15 degrees longitude) smoothed Odin column data (back stars). The retrieved CO from Odin/SMR measurements were summed over the same grid as the gb-FTS one, from 24 km to 100 km using the method outlined in section 2.2. The entire Poker Flat gb-FTS data set covering the time period from February 2004 to June 2004 consists of 48 data points and shows the now established winter maximum, summer minimum reported earlier by *Kasai et al.* [2005b]. This seasonal trend is very closely followed by the 55 Odin data points (all available Odin data within the spatial criteria stated above in 2004) that are spread relatively evenly across the year. All data were recorded in polar daylight.

[22] In Figure 4, top, the color-coded gb-FTS symbols, in a similar fashion to Figure 3, represent MPV values, computed with data from the UK Meteorological Office.

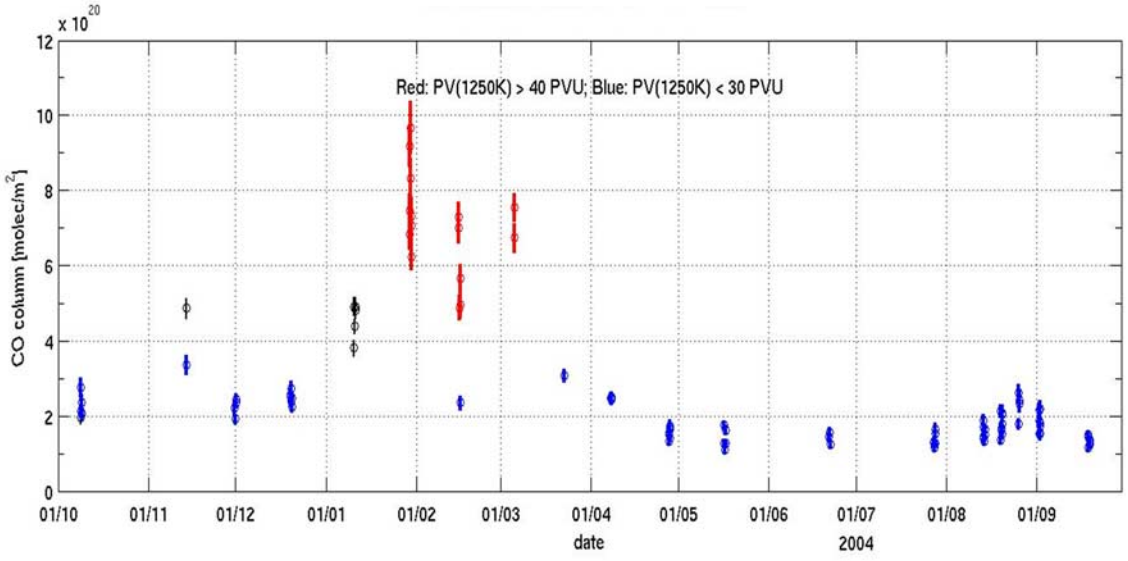

Figure 3. Available Odin/SMR data from October 2003 to September 2004 plotted with a color code to indicate the data proximity to the polar vortex on the 1250 K potential temperature surface: (red (>40 PVU)) inside the vortex, (black (<40 and >30 PVU)) in the collar region, and (blue (<30 PVU)) outside the polar vortex. Data are individual smCO partial columns measurements that have not been smoothed by the gb-FTS averaging kernels.

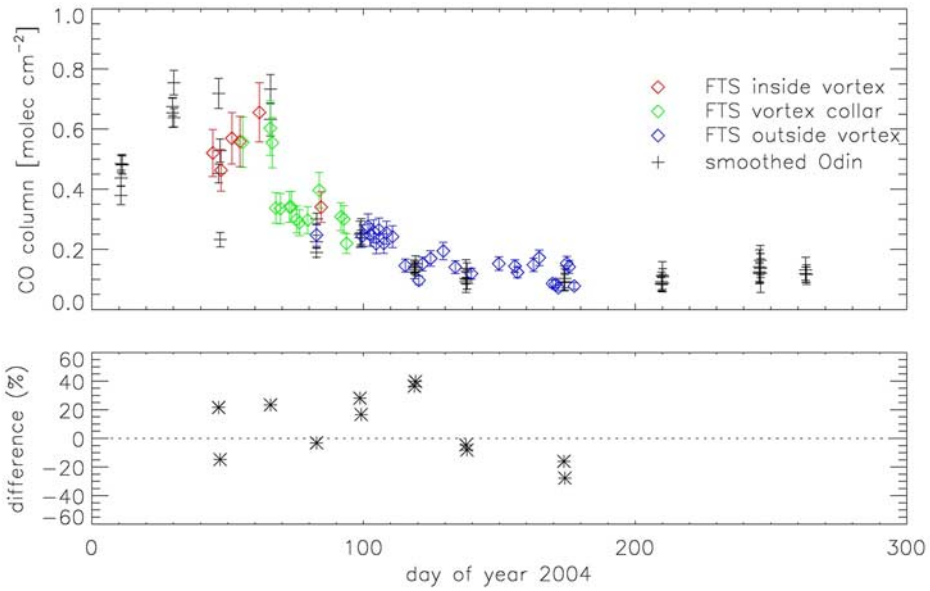

Figure 4. (top) A comparison of smCO partial column amounts from gb-FTS over the height range from 24–100 km and the Odin/SMR instrument (smoothed by the gb-FTS averaging kernel) for 2004. Colocation criteria used was ±5° latitude and ±15° longitude. Color code for the gb-FTS data (diamonds) reflects whether the measurements at Poker Flat were inside (red), in the collar (green), or outside (blue) the polar vortex based on the 1250 K potential temperature surface. (bottom) Relative percentage difference, $(\tilde{C}_{fo} - C_{FTS})/\bar{C}_{FTS} \times 100$, where $\tilde{C}_{fo}$ is the smoothed Odin/SMR CO partial column from equation (1), C_{FTS} is the gb-FTS CO partial column interpolated onto the Odin/SMR time grid, and $\bar{C}_{FTS}$ is the mean gb-FTS CO partial column for periods chosen on the basis of whether the Poker Flat mesosphere (1250 K surface) was inside, in the collar, or outside the polar vortex (see section 3.3 for a description of these time periods).

Because of Poker Flat's proximity to the Arctic vortex in winter, the dynamics of the vortex means that the Poker Flat upper stratosphere in particular (from the 1250 K potential temperature data), is inside the vortex during winter, in the collar region during spring, and then outside the vortex for the rest of the year. We have therefore used the method of *Nash et al.* [1996], where the location of the vortex edge is defined by the maximum gradient in the PV as a function of equivalent latitude. In this section we use the 1250 K surface and use MPV (equation (3)) to determine whether this value is within the vortex (MPV > 40 PVU), within the collar region (30 < MPV < 40 PVU), or outside the vortex (MPV < 30 PVU). These three regimes have been color coded in Figure 4 as follows; red inside the vortex, green the collar, and blue for outside the vortex. Later in section 3.7 we examine the gb-FTS data as a function of equivalent latitude. Also plotted in Figure 4, bottom, is the percentage difference: $(\tilde{C}_{fo} - C_{FTS})/\bar{C}_{FTS} \times 100$, where $\tilde{C}_{fo}$ is the smoothed Odin/SMR smCO partial column from equation (1), C_{FTS} the gb-FTS smCO partial column interpolated onto the Odin/SMR time grid, and $\bar{C}_{FTS}$ the mean gb-FTS smCO partial column for periods chosen on the basis of whether the Poker Flat upper stratosphere-mesosphere (1250 K surface) was inside, in the collar, or outside the polar vortex. The interpolated gb-FTS smCO partial column, C_{FTS}, was computed by using a parametric cubic spline interpolation scheme that allowed the use of randomly placed time points, which were subsequently resampled onto a fine 1 h grid. From this finely interpolated gb-FTS data, points were then chosen to exactly match the Odin/SMR data points. Since the gb-FTS data are daily means, for this particular exercise of comparing their differences, we have used daily mean smoothed Odin data. In doing so, we are able to directly compare all gb-FTS data with the 12 daily mean smoothed Odin/SMR 2004 data values. The percentage differences (Figure 4, bottom) are scattered about zero, with a mean difference of 7.6 ± 6%, i.e., a small positive bias but not significant within the uncertainties of both measurements. A few individual data points in Figure 4, bottom, do exceed 30%, but these generally occur during the summer period where the absolute amounts of CO are relatively low. To investigate this small bias, a simple T-test on the two data sets (12 Odin/SMR values and the 12 sampled/interpolated gb-FTS data points), gives a T paired value of 1.07 for 11 degrees of freedom; that is, the two sample means are not statistically different. The squared correlation coefficient, r^2, is 0.91, also indicating that the two data sets are well correlated.

[23] There is excellent agreement between the CO measurements from two quite different techniques, one with upward looking geometry in solar absorption, and the other with limb geometry in emission from space, suggesting that the Poker Flat gb-FTS can offer reliable CO measurements

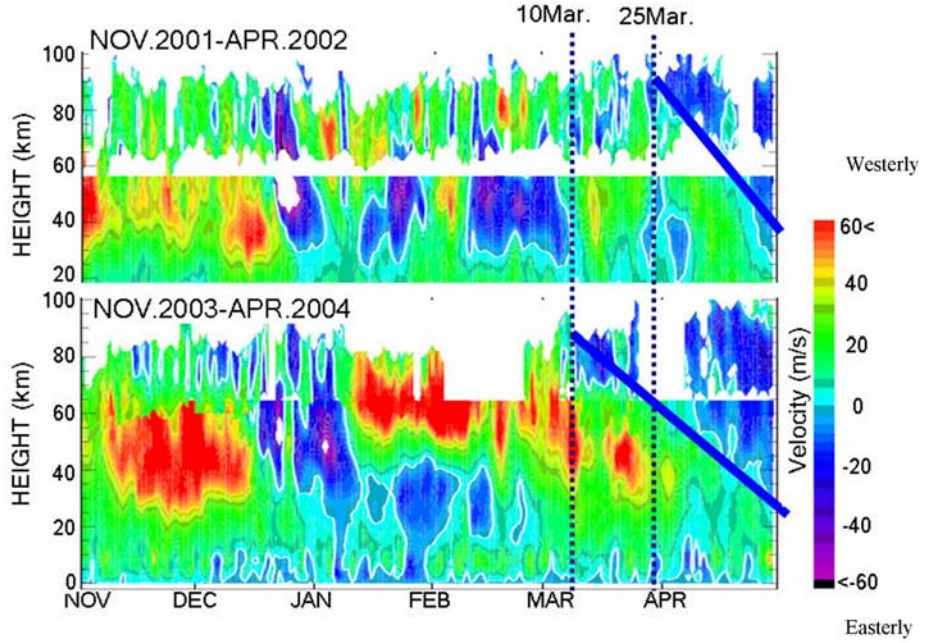

Figure 5. Zonal wind contours of Poker Flat MF radar data (60 km and above) and UK Met Office (UKMO) (below 60 km) for 2002 and 2004. Wind direction is indicated by color (blue: westerly (−), red: easterly (+)).

in the middle and upper atmosphere in conjunction with the Odin/SMR instrument.

3.4. Poker Flat MF Radar

[24] Figure 5 shows zonal wind contours of Poker Flat MF radar data (60 km and above) and UK Met Office (UKMO) (below 60 km) for 2002 and 2004. The color coding is indicated on the side bar of Figure 5; easterly winds are green-yellow-red, while westerly winds are represented by blue-magenta, both color schemes running weak to strong. It is assumed that the general behavior of large-scale mesospheric wind structures with long timescales of orders of a month can be represented by a single-site observation. This assumption, especially for zonal wind measurements, is supported by comparisons between Poker Flat and Andenes (Sweden, 69°N, 16°E) radar winds which show variations reasonably similar to each other over long timescales (plots not shown). Since meridional circulation from the South to North Pole in the mesosphere is driven by gravity wave-induced deceleration of the zonal mean flow, a change in the observed mean zonal wind direction from winter (westerly wind) to summer (easterly) may be used as a measure of the winter-to-summer transition of meridional transport of trace gases. Direct use of the observed meridional wind would be preferable, but the dominant planetary wave during winter disturbs the meridional winds (which is generally very much weaker than zonal wind). Zonal winds are also disturbed by planetary waves, but the zonal wind strength can be used as a measure of the dominant zonal jet strength, which in turn is related to global-scale dynamics.

[25] Figure 5, bottom, shows the 2003–2004 winter. The green-yellow-red color tends to dominate the 2003–2004 winter mesosphere, that is, westerly winds dominate in the middle atmosphere, indicating a winter middle atmosphere jet (likely coupled with the stratospheric polar vortex).

[26] Subsequently, in early March at 70–80 km, the westerly winds (yellow-green) reversed direction to easterly (blue). This is followed by wind reversal at lower heights, likely leading to the winter-to-summer transition in the circulation pattern in the middle atmosphere. This means in early March 2004, the winter pattern started to weaken in the mesosphere. The meridional circulation, which is assumed to transport CO poleward and downward in the stratosphere-mesosphere, weakened, resulting in the decline of CO transported from the upper and midlatitude regions. In April, the winter pattern seems to continue to weaken, and a clearer summer pattern emerges in the mesosphere and gradually penetrates downward in the stratosphere.

[27] Looking at the 2001–2002 winter data in Figure 5, top, the zonal wind reversal of winter-summer pattern transition started later, approximately 25 March 2002, as indicated by the thick blue line in Figure 5. Up to this point in time in the mesosphere and stratosphere, the green color or moderate westerly wind was predominant, except for a couple of blue regions or easterly winds. This may suggest stratospheric sudden warming events, which are defined when the mean zonal winds at 60°N and 10 hPa become easterly during winter [*Charlton and Polvani*, 2007]. Two such events have been reported during the 2001–2002 winter (http://www.appmath.columbia.edu/ssws/); 30 December 2001 and 17 February 2002.

[28] Comparing the 2002 and 2004 March wind reversal time in the Arctic mesosphere, the winter pattern of poleward and downward winds seemed to weaken earlier

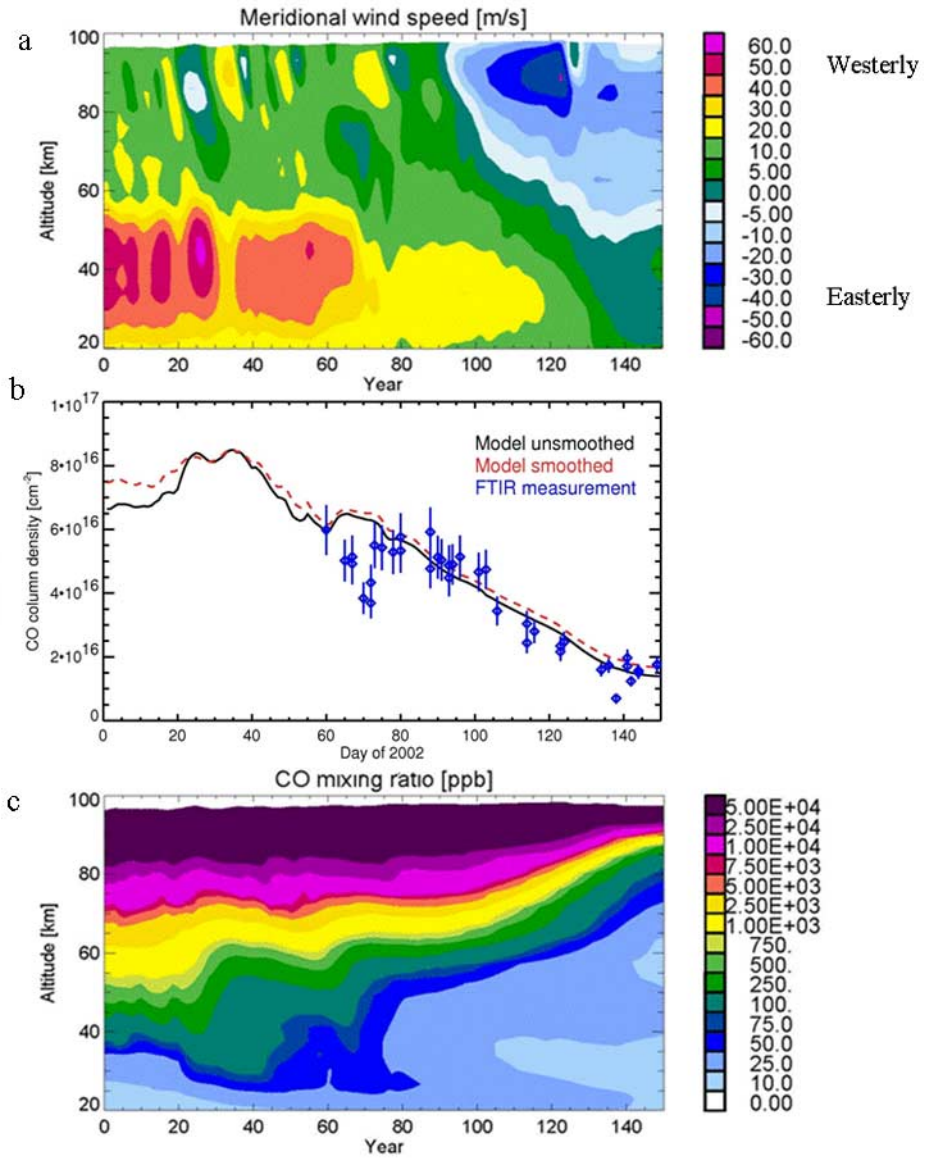

Figure 6. Two-dimensional Leeds-Bremen model of zonal longitudinally averaged Poker Flat stratospheric/mesospheric (a) wind speeds, (b) model smCO partial columns (red dashed line) and model smCO partial columns smoothed with the gb-FTS averaging kernel (black line) calculated on the gb-FTS vertical grid, and (c) CO mixing ratio for 2002. Also plotted on Figure 6b, blue diamonds are the gb-FTS partial columns with error bars.

in 2004 than in 2002, resulting in less CO transport from the source region. This scenario can explain long-term trends like, for example, seasonal progression or month-to-month variability, but is not applicable to shorter-term variation like polar vortex motion around the pole over 10 d or so.

[29] This difference in wind reversal is also consistent with the fitted phase difference between years 2002 and 2004 of 30 ± 11 d in the CO stratomesospheric column reported in section 3.1. The determination of the difference in dates of the wind reversal in this current work of approximately 15 d was not quantitative, but based on a qualitative assessment of the wind gradients. It does indicate however that this was most likely the driving mechanism of the phase difference in the CO stratomesospheric columns.

3.5. Two-Dimensional Leeds-Bremen Model

[30] Results for 2002 from the modified Leeds-Bremen model that includes thermospheric CO is shown in Figure 6 which examines the proposed meridional wind-CO column relation. In this study we have used derived zonal winds that are relatively straightforward to derive from the model output. There are several factors why we have used zonal winds as a proxy for the meridional circulation, which was also discussed in section 3.4 with respect to the MF radar zonal wind data. First the computation of meridional winds

from model output is very complex. Secondly, in general the zonal wind is much stronger and more stable than the meridional wind especially in the mesosphere, so the use of the zonal wind is a better index of global-scale dynamic features than the meridional component. Thirdly, from an observation point of view, it is considered very difficult to identify a suitable measure of the global-scale meridional flow. Instead, the meridional wind data shows more short-term and/or smaller-scale variability such as atmospheric waves (particularly planetary waves). On the other hand, the zonal component is a more stable reflection of global-scale behavior because the jet structure, which dominates the northern middle to high latitudes, is the source of the strong and predominant zonal winds. Finally, when the polar vortex is shifted off-pole, the weaker meridional wind often changes direction between southerly to northerly in terms of the relative position of the Poker Flat observatory to the polar vortex center, especially for the cases when the planetary waves (zonal wave numbers 1 and/or 2) are dominant. For the zonal wind, even if the vortex is shifted, the zonal flow is more or less in the same direction in many cases. The zonal flow can therefore be used as an index or a measure of the jet structure over the northern mid-to-high-latitude region (sudden stratospheric warmings are exceptions though).

[31] In Figure 6 there are three panels labelled 6a (model mean longitudinally averaged zonal wind fields), 6b (model and gb-FTS stratomesopheric partial columns), and 6c (model CO mixing ratios). The model was run over other years as well (not shown), but did not show significant interannual variability. This lack of year-to-year variation in the model is due to the use of a single year of Eliassen-Palm (EP) fluxes to drive the circulation. Model results have also been smoothed to the vertical resolution of the gb-FTS measurements using the same method for smoothing the Odin/SMR data via equation (1).

[32] The decrease of the CO column, starts at around day 80 (Figure 6b), with the transition to continuously "blue" (easterly) wind speeds (6a) starting around day 90 (at approximately 90 km); on closer inspection, the zonal circulation starts to weaken by day 75 (from 70 to 90 km), slightly before the decline in the CO column. We also note that the absolute value of the CO column above 24 km (peak of $6-7 \times 10^{16}$ and a minimum of $1-2 \times 10^{16}$ molec cm^{-2}) and the seasonal trend from the model and the gb-FTS measurements (Figure 6b) are quite consistent. Generally, there is considerable variability in both the model CO column and wind fields between days 0 and 80. Afterward, the model CO column decreases systematically while the wind field changes to strong easterlies. The downward trend in the gb-FTS columns is not clear, within the error bars, until after about day 100. One could also interpret the model CO column as having two maxima, around day 30 and day 70, decreasing from day 70 onward. The latitude of the Poker Flat site is such that it is normally just outside the Arctic polar vortex (at least in the stratosphere, this is not the case for the winter mesosphere, see section 3.7). Any decrease in CO can be caused by air masses that are affected by sunlight (by the reaction CO + OH), which might also coincide with the circulation as well. If the meridional circulation breaks down, the polar vortex weakens or disappears altogether so that mixing with midlatitude (rich in OH and low in CO) stratospheric air is possible. For the gb-FTS data in particular, the smCO partial column cannot distinguish between the stratosphere and mesosphere, so the variability could be either driven by chemistry in the stratosphere, lower mesosphere, or transport in the upper mesosphere.

[33] If we compare the details of the model zonal wind fields, Figure 6a, with the zonal wind MF radar data (Figure 5) there are clearly differences. This is to be expected as the single point radar data and longitudinally averaged model data are representing slightly different aspects of the general circulation. In the winter stratosphere-mesosphere, both the zonal and meridional winds are highly variable (on multiple temporal scales, i.e., day-to-day, month-to-month, and even year-to-year) and are significantly affected by tropospheric weather systems. Year-to-year variability is particularly strong, so the use of a fixed EP flux in the model (which represents planetary Rossby waves) precludes any meaningful discussion here about year-to-year differences from model data. The direction of the meridional wind at the Poker Flat site in the lower to middle stratosphere also depends on the relative position of the polar vortex. The purpose here is to show that there is agreement in the absolute CO partial columns and overall seasonal dependence between the ground-based data and model calculations. While we have used zonal winds as a proxy for meridional flow, the longer-term seasonal agreement shows that this is a reasonable assumption.

3.6. The 2003–2004 Arctic Winter

[34] The Arctic Winter of 2003–2004 displayed the most unusual stratospheric warming event on record for the Northern Hemisphere [*Manney et al.*, 2005]. Detailed analysis of the meteorological fields show that in early December 2003 the upper stratospheric polar vortex broke up, recovering in February–March 2004 to be the strongest on record. Throughout the stratosphere there were unusually high temperatures and low zonal wind speeds that disrupted the polar vortex for about 2 months [*Manney et al.*, 2005]. These reports are completely consistent with the MF radar data (Figure 5, bottom) which show strong easterly winds in the upper stratosphere in December 2003, to be replaced by weak easterly winds throughout the stratosphere and mesosphere. Throughout January and February strong easterly winds dominate throughout the stratosphere, consistent with the polar vortex being reestablished. As well as having significantly higher upper stratosphere temperatures, the 2003–2004 Arctic Winter stratosphere also had anomalously high ozone compared with previous values in the 1980s (http://www.cpc.noaa.gov/products/stratosphere/winter_bulletins/nh_03-04/). In early March, while there are still easterly winds in the stratosphere, the mesosphere (Figure 5, bottom), has turned westerly, the beginning of the decline in measured stratomesospheric CO columns.

3.7. Dynamics of 2002 and 2004 Arctic Winters

[35] Figures 7, 8, 9, and 10 show the effects of differences in air mass history on the CO column by comparing the CO column amount with the Modified Potential Vorticity as defined in equation (3), section 3.3, for the 1250 K (Figures 7 and 8, 2002 and 2004, respectively) and 900 K

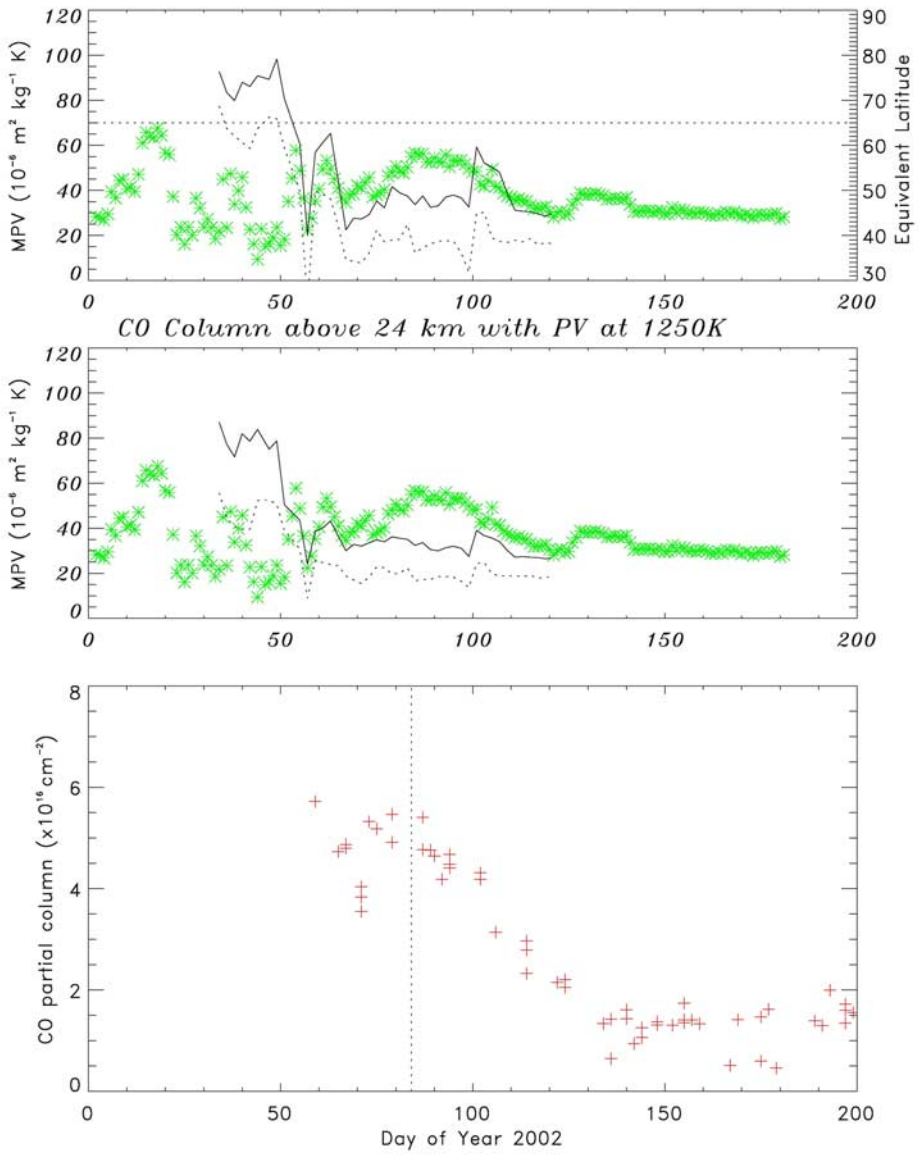

Figure 7. (top) Modified Potential Vorticity (MPV) (left waxis, green stars) on the 1250 K potential temperature surface (upper stratosphere) using UKMO data for Poker Flat, 2002, plotted with equivalent latitude (right axis, solid line vortex – collar boundary, dashed line vortex collar – edge boundary). Horizontal dashed line is the latitude of Poker Flat for reference. (middle) Same MPV data as above for the Poker Flat location, but with the solid line now representing the MPV of the vortex inner collar, and the dashed line representing the vortex edge. (bottom) The smCO partial column (red crosses) for reference including the vertical dashed line for the first date marked from Figure 5, i.e., 10 March 2002.

(Figures 9 and 10, 2002 and 2004, respectively) potential temperature surfaces. All four figures have the following features: the top panels in each figure show the MPV on the left axis and are marked with green stars, while the right axis of the top panels indicate the equivalent latitude plotted as black solid and dotted lines for the inner and outer edge of the polar vortex (using temperature and wind fields from the UKMO assimilated data as before). The middle panel of each of Figures 9 and 10 is the MPV for Poker Flat as in the top panel (green stars), but the black solid and dotted lines are the MPV of the inner and outer vortex edge. Finally, the bottom panel is the gb-FTS stratomesospheric CO partial column for reference.

[36] Starting with Figure 7, top, which is the MPV (1250 K), and equivalent latitude for 2002, we see that soon after day 50, the Poker Flat upper stratosphere-mesosphere is within the polar vortex, and subsequently the CO stratomesospheric CO column is high. This remains the case until sometime after day 100 when the polar vortex weakens and it becomes difficult for the Nash method to determine where the vortex edge is. In Figure 8, top, the Poker Flat upper stratosphere-mesosphere remains marginally inside the

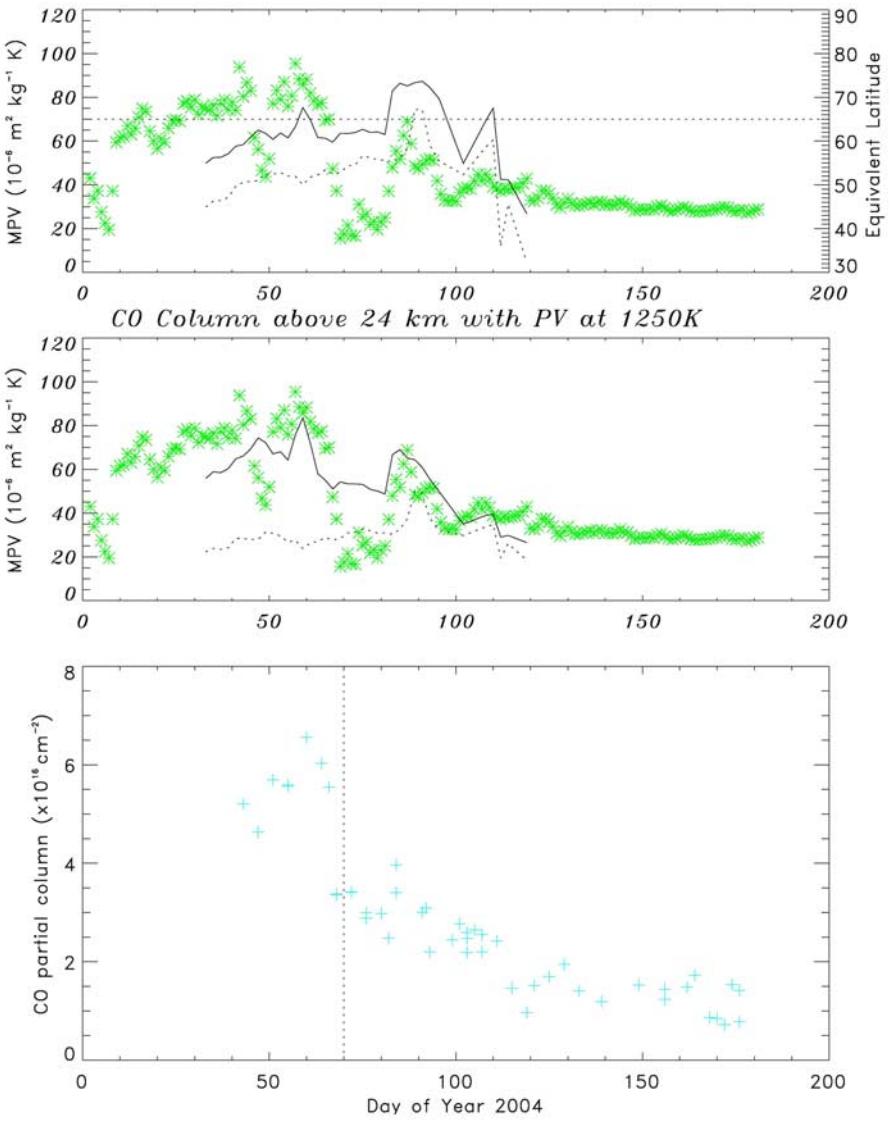

Figure 8. (top and middle) Same as Figure 7 except the results are for 2004; (bottom) 2004 smCO partial columns (blue crosses).

polar vortex until day 70, when the MPV values dramatically drop at the same time as the CO stratomesospheric CO column. The upper stratosphere-mesosphere above Poker Flat does not strictly move outside the polar vortex, on the basis of equivalent latitude until 10 d later on day 80. The vertical dashed line in the CO column plot is the transition date of 10 March and 25 March for 2002 and 2004, respectively, from westerly to easterly zonal winds in the upper mesosphere as shown in Figure 5.

[37] The situation for the 900 K potential temperature surface, as indicated in Figures 7–10, is around 30 km (middle stratosphere), is somewhat different. The MPV for 2002 is highly variable up to day 130 where it settles down to a summer value of around 30 MPV Units. During the winter/spring period of 2002, the MPV remains at or above 40 PVU, averaging close to 50 PVU. However in terms of equivalent latitude, the Poker Flat upper stratosphere remains outside the polar vortex throughout the entire winter/spring period. Occasional low MPV values on day 84, 110, and 130 correspond to an approximate 25% decline in the CO column. In Figure 10, however, we see a slightly more dramatic situation with the 2004 MPV values corresponding to an abrupt change in the CO column. Again, the 2004 winter/spring PV values are in general highly variable, except that on day 70 (10 March) the PV returns to typical summer values of 30 PVU, remaining at this value for nearly 2 weeks. Further, the Poker Flat upper stratosphere is in the vortex collar region up to the transition date of 10 March. Consequently, the CO column drops more than 40%. Despite the PV returning to higher values for brief periods of time after day 90, the CO column never recovers, slowly decreasing to summer amounts over the next 50 d.

[38] Collectively, Figures 7 through 10 illustrate that the most likely dynamical driving mechanism in the gb-FTS

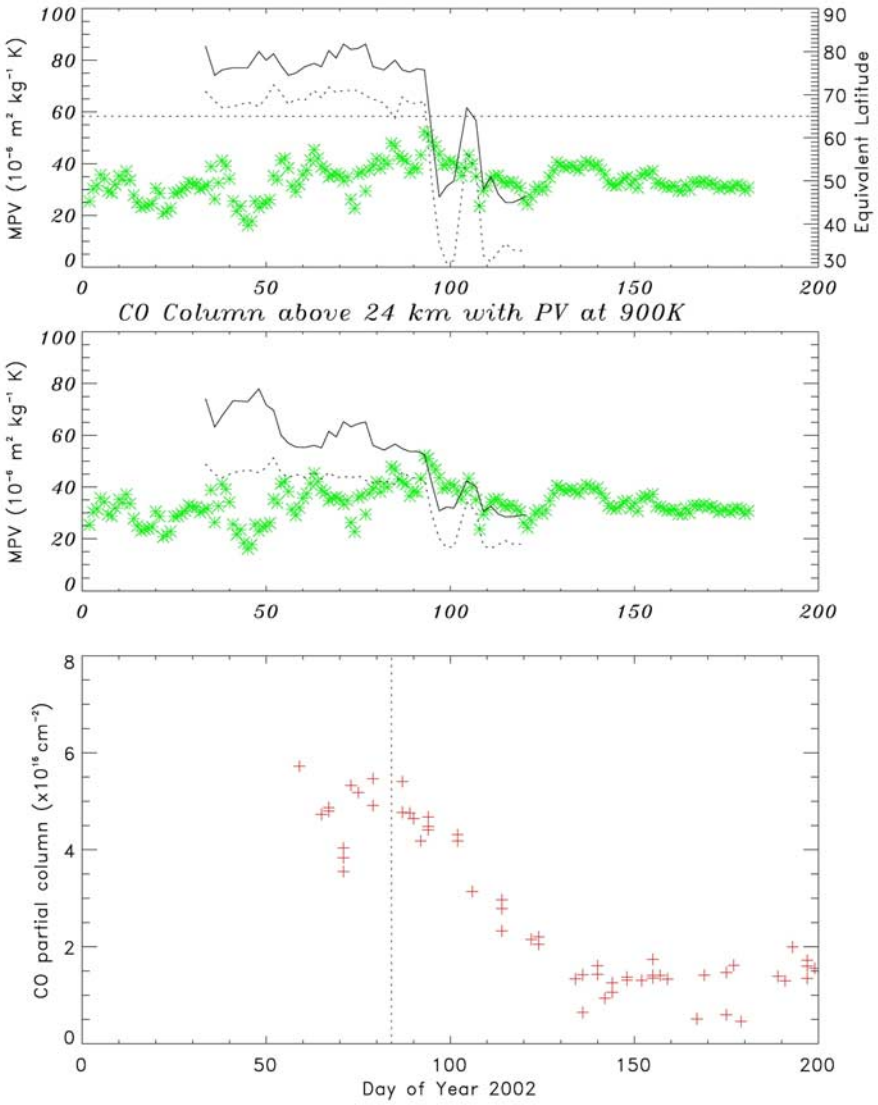

Figure 9. (top) MPV (left axis, green stars) on the 900 K potential temperature surface (middle stratosphere) using UKMO data for Poker Flat, 2002, plotted with equivalent latitude (right axis, solid line vortex: collar boundary, dashed line vortex collar: edge boundary). Horizontal dashed line is the latitude of Poker Flat for reference. (middle) Same MPV data as above for the Poker Flat location, but with the solid line now representing the MPV of the vortex inner collar, and the dashed line representing the vortex edge. (bottom) The smCO partial column (red crosses) for reference including the vertical dashed line for the second date marked from Figure 5, i.e., 25 March 2002.

column data is the mesosphere, as this part of the vertical structure of the atmosphere is mostly within the winter polar vortex in the 2 a we have studied closely. This is closely supported by Odin/SMR data in terms of the dynamics and seasonal trends in the CO stratomesospheric columns.

4. Conclusions

[39] Stratomesospheric CO has been reported from Poker Flat, Alaska, from mid-IR data recorded by a gb-FTS. Five years of data (2000 to 2004) were presented which showed a number of interesting features. All 5 a of data have very high (factor of 6 above midsummer values) winter maxima. The 2004 year was unusual, compared with the other years in the study, as the transition from winter to summer CO values in the mesosphere occurred 1 month early (30 ± 11 d), however, on six occasions in March of 2002 (between the 6th and 15th), the mesospheric partial column followed the 2004 pattern rather than the more general trend of the other years. Poker Flat is situated at the edge of the stratospheric polar vortex in winter, but because of dynamical changes in the circulation patterns it is sometimes

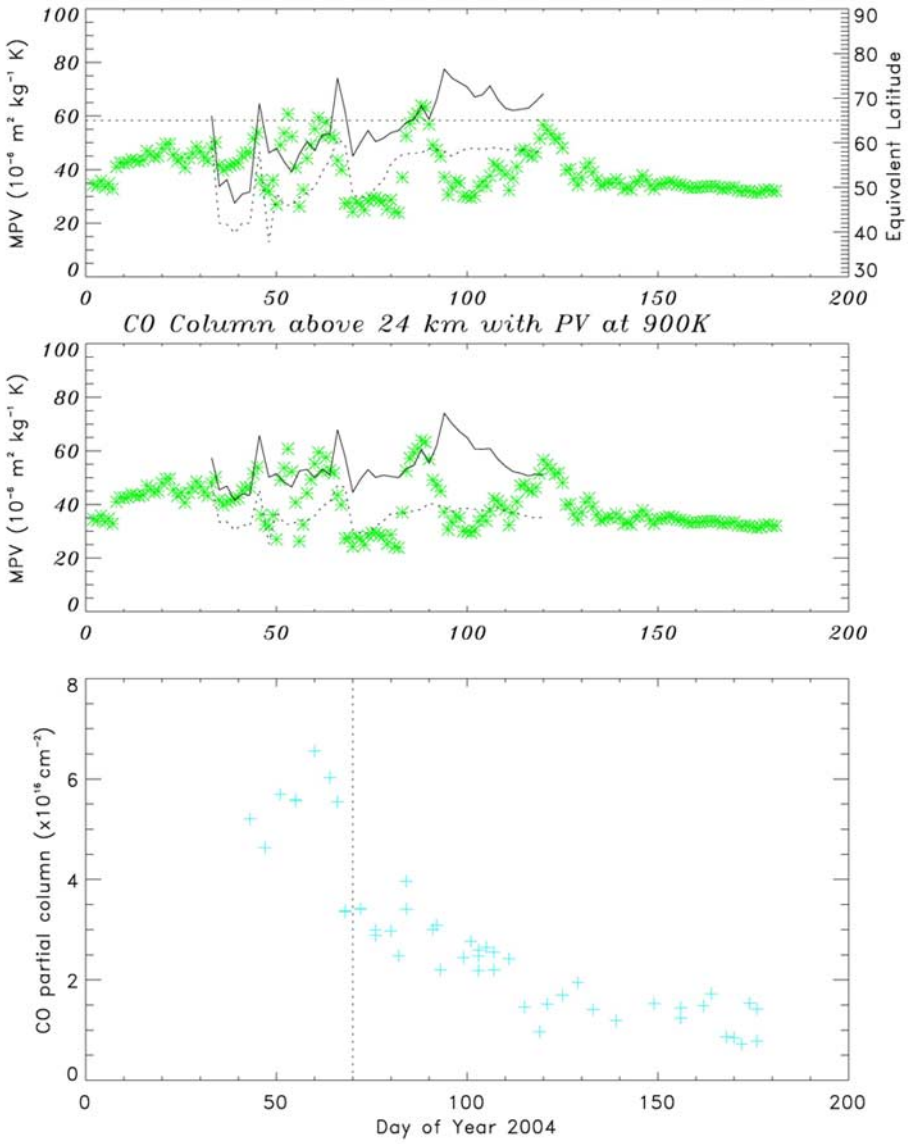

Figure 10. (top and middle) Same as Figure 9 except the results are for 2004; (bottom) 2004 smCO partial columns (blue crosses).

within the vortex; this occurred on 20 March 2001 where the highest measured CO partial column occurred (8.5×10^{16} molec cm^{-2}). By late October the mesospheric circulation has returned to its normal winter pattern based on the latest recorded CO partial column in anyone year (24 October 2002). PV values on the 1250 K potential temperature surface (40 km) in equivalent latitude coordinates clearly indicated that the upper stratosphere-mesosphere above Poker Flat was within the polar vortex for most, if not of all the Arctic winter periods studied.

[40] The ground-based data were compared with satellite data from the Odin/SMR instrument. The satellite data, at a much higher vertical resolution than the ground-based data were smoothed with the gb-FTS averaging kernel, and on that basis were found to agree to within the error limits. That is, for a limited number of colocated days (12) the mean difference between the data sets was found to be 8 ± 6%, with a correlation r^2 of 0.91. While the number of data points in this initial comparison was limited to only 12 d, the significant differences in the measurement techniques, platforms and geometry make the agreement between the two data sets particularly pleasing. Further work on these data is planned as the Odin/SMR data set continues to accumulate.

[41] Comparison with a 2-D chemical transport model also showed good agreement with the gb-FTS partial column amounts, within the measurement uncertainties, in both absolute amounts and seasonal dependence for 2002.

[42] Finally, data from a colocated zonal wind radar indicated that the year-to-year variability in the CO partial

column could be explained in terms of mesospheric wind dynamics. In particular, the radar data indicated that 2004 was influenced by the early breakdown of the winter polar circulation. This is supported by PV data as described earlier with respect to the upper stratosphere-mesosphere above Poker Flat, as well as other studies that showed the unusual stratospheric warming that occurred in the 2003/2004 Arctic winter. In 2004 the upper stratosphere displayed typical summer values of 20 PVU for nearly 2 weeks, about 1 month (30 ± 11 d) earlier than other years. Components of the 2002 data also followed the 2004 pattern, but returned to the dynamical characteristics of the other years (2000, 2001, and 2003) in the late winter period. We caution however, that these conclusions on the smCO partial column and its relationship with large-scale circulation patterns are based on measurements from a single ground station. Work on other CO data sets, including space-based measurements is continuing.

[43] **Acknowledgments.** Support of the Australian Research Council is gratefully acknowledged as well as funding from the National Institute for Communications Technology through the Alaska Project. We thank the UK Meteorological Office for the use of data for PV calculations.

References

Aellig, C. P., N. Kämpfer, and A. Hauchecorne (1995), Variability of mesospheric CO in the fall and winter as observed with ground-based microwave radiometry at 115 GHz, *J. Geophys. Res.*, *100*, 14,125–14,130.

Ahmad, S. P., J. W. Waters, J. E. Johnson, I. V. Gerasimov, G. G. Leptoukh, and S. J. Kempler (2006), Atmospheric composition data products from the EOS Aura MLS, paper presented at The 86th AMS Annual Meeting, Eighth Conference on Atmospheric Chemistry, Am. Meteorol. Soc., Atlanta, Ga., 28 January to 3 February.

Allen, D. R., J. L. Stanford, M. A. Lopez-Valverde, N. Nakamura, D. J. Lary, A. R. Douglass, M. C. Cerniglia, J. J. Remedios, and F. W. Taylor (1999), Observations of middle atmosphere CO from the UARS ISAMS during the early northern winter 1991/92, *J. Atmos. Sci.*, *56*(4), 563–583.

Barret, B., S. Turquety, D. Hurtmans, C. Clerbaux, J. Hadji-Lazaro, I. Bey, M. Auvray, and P.-F. Coheur (2005), Global carbon monoxide vertical distributions from spaceborne high-resolution FTIR nadir measurements, *Atmos. Chem. Phys. Disc.*, *5*, 4599–4639.

Barret, B., et al. (2006), Intercomparisons of trace gases profiles from the Odin/SMR and Aura/MLS limb sounders, *J. Geophys. Res.*, *111*, D21302, doi:10.1029/2006JD007305.

Bevilacqua, R. M., A. A. Stark, and P. R. Schwartz (1985), The variability of carbon monoxide in the terrestrial mesosphere as determined from ground-based observations of the J = 1–0 emission line, *J. Geophys. Res.*, *90*, 5777–5782.

Bhattacharya, S. K., J. Savarino, and M. H. Thiemens (2000), A new class of oxygen isotopic fractionation in photodissociation of carbon dioxide: Potential implications for atmospheres of Mars and Earth, *Geophys. Res. Lett.*, *27*, 1459–1462.

Briggs, B. H. (1984), *The Analysis of Spaced Sensor Records by Correlation Techniques*, pp. 166–186, Univ. of Illinois, Urbana, Ill.

Charlton, A. J., and L. M. Polvani (2007), A new look at stratospheric sudden warmings. part I: Climatology and modeling benchmarks, *J. Clim.*, *20*(3), 449–469.

Chipperfield, M. P. (1999), Multiannual simulations with a three-dimensional chemical transport model, *J. Geophys. Res.*, *104*, 1781–1805.

Clerbaux, C., P.-F. Coheur, D. Hurtmans, B. Barret, M. Carleer, R. Colin, K. Semeniuk, J. C. McConnell, C. Boone, and P. Bernath (2005), Carbon monoxide distribution from the ACE-FTS solar occultation measurements, *Geophys. Res. Lett.*, *32*, L16S01, doi:10.1029/2005GL022394.

Dowdy, A., R. A. Vincent, K. Igarashi, Y. Murayama, and D. J. Murphy (2001), A comparison of mean winds and gravity wave activity in the northern and southern polar MLT, *Geophys. Res. Lett.*, *28*, 1475–1478.

Dupuy, É., et al. (2004), Strato-mesospheric measurements of carbon monoxide with the Odin Sub-Millimetre Radiometer: Retrieval and first results, *Geophys. Res. Lett.*, *31*, L20101, doi:10.1029/2004GL020558.

Forkman, P., P. Eriksson, A. Winnberg, R. R. Garcia, and D. Kinnison (2003), Longest continuous ground-based measurements of mesospheric CO, *Geophys. Res. Lett.*, *30*(10), 1532, doi:10.1029/2003GL016931.

Forkman, P., P. Eriksson, D. Murtagh, and P. Espy (2005), Observing the vertical branch of the mesospheric circulation at latitude 60°N using ground-based measurements of CO and H_2O, *J. Geophys. Res.*, *110*, D05107, doi:10.1029/2004JD004916.

Iishi, M. S. O., E. Sagawa, Y. Murayama, S. Watari, M. Conde, and R. W. Smith (2000), Development of CRL Fabry-Perot interferometers and observation of the thermosphere, *Rev. Commun. Res. Lab.*, *48*(2), 155–164.

Jin, J. J., et al. (2005), Co-located ACE-FTS and Odin/SMR stratospheric-mesospheric CO 2004 measurements and comparison with a GCM, *Geophys. Res. Lett.*, *32*, L15S03, doi:10.1029/2005GL022433.

Kasai, Y., T. Koshiro, M. Endo, N. B. Jones, and Y. Murayama (2005a), Ground-based measurement of strato-mesospheric CO by a FTIR spectrometer over Poker Flat, *Alaska, Adv. Space Res.*, *35*, 2024–2030.

Kasai, Y. J., A. Kagawa, N. Jones, A. Fujiwara, K. Seki, Y. Murayama, and F. Murcray (2005b), Seasonal variations of CO and HCN in the troposphere measured by solar absorption spectroscopy over Poker Flat, Alaska, *Geophys. Res. Lett.*, *32*, L19812, doi:10.1029/2005GL022826.

Kinnersley, J. S. (1996), The climatology of the stratospheric THIN AIR model, *Q. J. R. Meteorol. Soc.*, *122*, 219–252.

Lait, L. R. (1994), An alternative form for potential vorticity, *J. Atmos. Sci.*, *51*, 1754–1759.

López-Valverde, M., J. J. Remedios, C. D. Rodgers, F. W. Taylor, E. C. Zipf, and P. W. Erdman (1996), Validation of measurements of carbon monoxide from the improved stratospheric and mesospheric sounder, *J. Geophys. Res.*, *101*, 9929–9955.

Manney, G. L., K. Kruger, J. L. Sabutis, S. A. Sena, and S. Pawson (2005), The remarkable 2003–2004 winter and other recent warm winters in the Arctic stratosphere since the late 1990s, *J. Geophys. Res.*, *110*, D04107, doi:10.1029/2004JD005367.

Müller, R., C. A. M. Brenninkmeijer, and P. J. Crutzen (1996), A large ^{13}CO deficit in the lower Antarctic stratosphere due to "ozone hole" chemistry: part II, Modeling, *Geophys. Res. Lett.*, *23*, 2129–2132.

Murayama, Y., K. Igarashi, D. Rice, B. Watkins, R. Collins, K. Mizutani, Y. Saito, and S. Kainuma (2000), Medium frequency radars in Japan and Alaska, for upper atmosphere observations, *IEICE Trans. Commun.*, *E83-B*, 1996–2003.

Murtagh, D., et al. (2002), An overview of the Odin atmospheric mission, *Can. J. Phys.*, *80*(4), 309–319.

Nash, E. R., P. A. Newman, J. E. Rosenfield, and M. R. Schoeberl (1996), An objective determination of the polar vortex using Ertel's potential vorticity, *J. Geophys. Res.*, *101*, 9471–9478.

Riggin, D. M., C. K. Meyer, D. C. Fritts, M. J. Jarvis, Y. Murayama, W. Singer, R. A. Vincent, and D. J. Murphy (2003), MF radar observations of seasonal variability of semidiurnal motions in the mesosphere at high northern and southern latitudes, *J. Atmos. Sol. Terr. Phys.*, *65*, 483–493.

Rinsland, C. P., N. B. Jones, B. J. Connor, A. Goldman, J. A. Logan, F. J. Murcray, T. M. Stephen, N. S. Pougatchev, R. Zander, P. Demoulin, and E. Mahieu (1998), Northern and Southern Hemisphere ground-based infrared spectroscopic measurements of tropospheric carbon monoxide and ethane, *J. Geophys. Res.*, *103*, 28,197–28,218.

Rodgers, C. D. (2000), *Inverse Methods for Atmospheric Sounding: Theory and Practice*, World Sci., London.

Rodgers, C. D., and B. J. Connor (2003), Intercomparison of remote sounding instruments, *J. Geophys. Res.*, *108*(D3), 4116, doi:10.1029/2002JD002299.

Rothman, L. S., A. Barbe, D. C. Benner, L. R. Brown, C. Camy-Peyret, M. R. Carleer, K. Chance, C. Clerbaux, V. Dana, and V. M. Devi (2003), The HITRAN molecular spectroscopic database: Edition of 2000 including updates through 2001, *J. Quant. Spectrosc. Radiat. Transfer*, *82*(1–4), 5–44.

Sinnhuber, M., J. Burrows, K. F. Künzi, M. P. Chipperfield, C. H. Jackman, M.-B. Kallenrode, and M. Quack (2003), A model study of the impact of magnetic field structure on atmospheric composition during solar proton events, *Geophys. Res. Lett.*, *30*(15), 1818, doi:10.1029/2003GL017265.

Solomon, S., R. R. Garcia, J. J. Olivero, R. M. Bevilacqua, P. R. Schwartz, R. T. Clancy, and D. O. Muhleman (1985), Photochemistry and transport of carbon monoxide in the middle atmosphere, *J. Atmos. Sci.*, *42*(10), 1072–1083.

Velazco, V., et al. (2007), Annual variation of strato-mesospheric carbon monoxide measured by ground-based Fourier transform infrared spectrometry, *Atmos. Chem. Phys.*, *7*, 1305–1312.

B. Barret and P. Ricaud, Laboratoire d'Aerologie, UMR 5560 CNRS/Universite Paul Sabatier, Observatoire de Midi-Pyrenees, 14, Avenue Edouard Belin, 31400 Toulouse, France.

E. Dupuy, Institute of Space and Atmospheric Studies, University of Saskatchewan, 116 Science Place, Saskatoon, SK, Canada S7N 5E2.

N. B. Jones, School of Chemistry, University of Wollongong, Wollongong, NSW 2522, Australia. (njones@uow.edu.au)

A. Kagawa, Y. Kasai, and Y. Murayama, Environmental Sensing and Network Group, Applied Electromagnetic Research Center, National Institute of Information and Communications Technology (NICT), 4-2-1, Nukui-Kitamachi, Koganei, Tokyo, 184-8795 Japan.

T. Koshiro, Research Institute for Sustainable Humanosphere, Kyoto University, Uji, 611-0011, Japan.

D. Murtagh and J. Urban, Department of Radio and Space Science, Chalmers University of Technology, Hörsalsvägen 11, SE-412 96 Gothenburg, Sweden.

M. Sinnhuber, Institute of Environmental Physics, University of Bremen, FB 1, Otto-Hahn-Allee 1, 28359 Bremen, Germany.